

Ultra-Precision Step Stage for Silicon Wafer Scanners

Bowen Zeng

Department of Mechanical Engineering

University of Michigan

E-mail: zbowen@umich.edu

Problem Being Solved

Ultra-precision scanning stages, comprising scanning and stepping axes, are used in advanced manufacturing equipment such as wafer scanners [1, 2]. The demand of microprocessor, whose substrate is silicon wafer, is predicated to increase in response to the development of big data, artificial intelligence, and internet of things (IoT) applications. Therefore, technologies that can increase the productivity and the quality of silicon wafers manufacturing should be continuously researched and developed. Since no useful process is done until the step stages reach target positions of the reference trajectory, step stages must deliver high (de)accelerations (e.g. $> 1 - 3$ g) during non-manufacturing portion of the trajectory to reduce waste-time. The resulting large inertial forces to boost throughput from linear motors cause Joule heating, which is proportional to the square of motor current (i.e., motor force) [3]. This heat generated from the motor is conducted to surrounding parts (e.g., table where silicon wafer is mounted), which reduce the positioning accuracy of the stage due to the thermal expansion. In addition, because the stage base is isolated from the ground by use of soft springs (i.e., pneumatic vibration isolators) to achieve desired precision during manufacturing [4], large reaction motor forces excite the softly sprung base, and unwanted residual vibration is created. Therefore, the stage must wait until the vibration gets settled to ensure the desired positioning precision [5]. In this report, an ultra-precision step stage design concept is presented, which can simultaneously mitigate the motor heating and stage vibration, while not compromising its positioning accuracy and throughput.

Scanning and Step Profile Used for Silicon Wafer Scanner

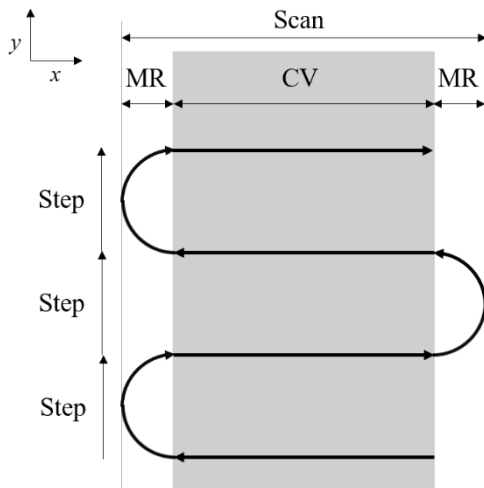


Figure 1.1. 2-D scanning profile

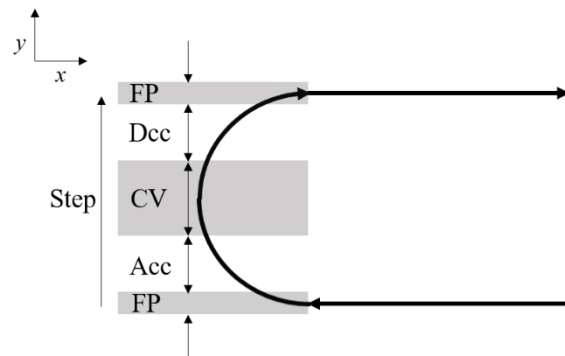


Figure 1.2. Regions of a step profile

Figure 1.1. shows a typical scanning profile used in a semiconductor manufacturing process. The y-axis advances in successive step motions while the x-axis scans repetitively [6]. Figure 1.2. shows a detailed step profile for a silicon wafer scanner. One step motion consists of an accelerating (Acc) region, an optional constant velocity (CV) region (depending on details of a reference trajectory), a decelerating (Dcc) region, and two fine positioning (FP) regions. Only at

those two fine positioning regions, high positioning accuracy is required to ensure accurate wafer scanning performances. Therefore, all other regions need to be executed as fast as possible with high (de)acceleration to reduce non-manufacturing time. During Acc and Dcc regions, motor actions create residual vibration to the isolated machine base, so it is important to reduce the magnitude of vibration, before the step stage works toward the precision-sensitive FP regions. Based on the characteristic step profile demonstrated in this section, a step stage design concept is generated that can simultaneously reduce motor heating and isolated base vibration. Following sections provide the design concept, prototype construction and performance evaluation.

Design Concept

Baseline Step Stage Model

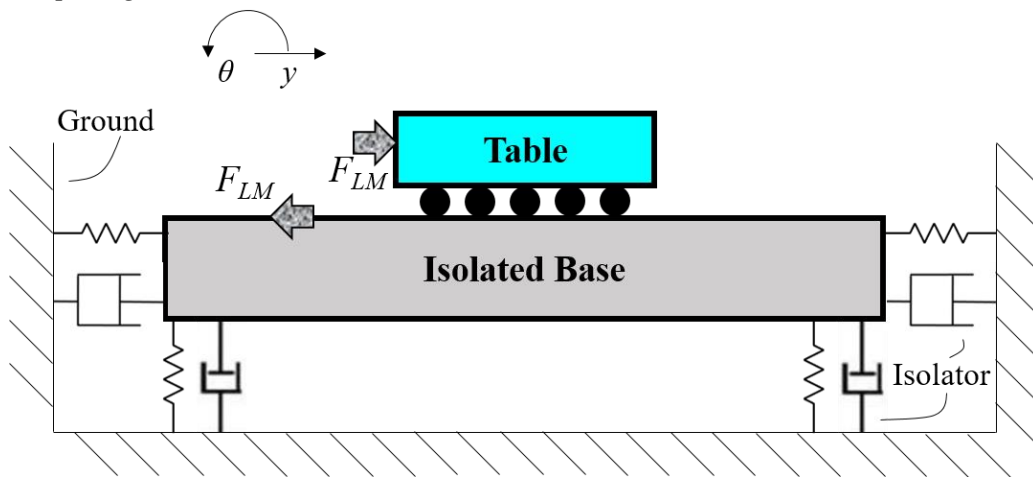


Figure 2. Baseline step stage model

To compare how the proposed step stage design concept can simultaneously reduce motor heating and stage vibration, a baseline step stage model is constructed for comparison, as shown in Figure 2. The table, driven by linear motor force, F_{LM} , is mounted on the isolated machine base. There are vibration isolators installed between the machine ground and the base, acting as soft springs, in order to filter the ground vibration to ensure highly precise fine positioning in FP regions. However, because of the presence of the vibration isolators, when the stage is (de)accelerating, unwanted horizontal (y) and rocking vibrations (θ) of the isolated base are created, resulting dwell time for waiting the entire stage to be settled down before conducting fine positioning in FP regions, and thus slowing down the wafer manufacturing process. In addition, even though linear motors have excellent fine positioning performance, it is energy-inefficient, so during Acc and Dcc regions, huge amount of unwanted heat is generated, resulting in thermal errors of the stage. The state space model of the baseline step stage model is given by:

$$\begin{bmatrix} \dot{y}_g \\ y_g \\ \dot{y}_b \\ y_b \\ \dot{y}_t \\ y_t \end{bmatrix} = \begin{bmatrix} 0 & -\frac{k_b + k_g}{m_g} & 0 & \frac{k_b}{m_g} & 0 & 0 \\ 1 & 0 & 0 & 0 & 0 & 0 \\ 0 & \frac{k_b}{m_b} & 0 & -\frac{k_b + k_p}{m_b} & 0 & \frac{k_p}{m_b} \\ 0 & 0 & 1 & 0 & 0 & 0 \\ 0 & 0 & 0 & \frac{k_p}{m_t} & 0 & -\frac{k_p}{m_t} \\ 0 & 0 & 0 & 0 & 1 & 0 \end{bmatrix} \begin{bmatrix} \dot{y}_g \\ y_g \\ \dot{y}_b \\ y_b \\ \dot{y}_t \\ y_t \end{bmatrix} + \begin{bmatrix} \frac{k_g}{m_g} \\ 0 \\ 0 \\ 0 \\ 0 \\ 0 \end{bmatrix} (y_v) \dots \text{Eq. (1)}$$

where y_g is the machine ground displacement, y_b is the isolated base displacement, y_t is the table displacement, y_v is the ground vibration input, m_g is the machine ground mass, m_b is the isolated base mass, m_t is the table mass, k_g is the ground stiffness, k_b is the equivalent isolator stiffness, and k_p is the equivalent stiffness between the stage and the base when the linear motor is operating.

Proposed Step Stage Design Concept

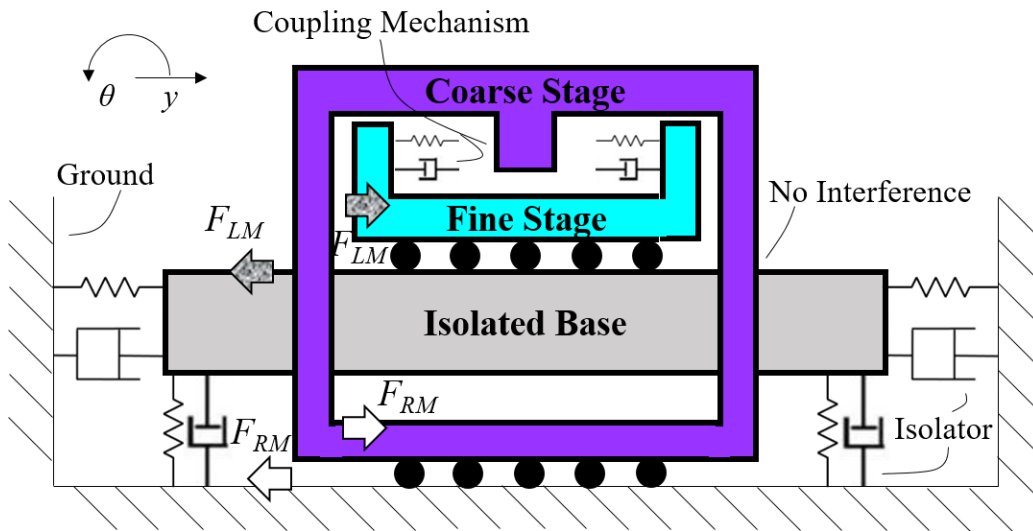


Figure 3. Proposed step stage design concept

The design concept of step stage for silicon wafer scanners is presented as shown in Figure 3. The step stage consists of two sub-stages: a coarse stage (CS) and a fine stage (FS). A silicon wafer is to be mounted on FS, so FS is directly mounted on the isolated machine base, in order to isolated the stage from ground vibrations. In the Acc, CV, and Dcc regions, FS is carried by the assistive CS via a coupling mechanism. The coupling mechanism has a male part and a female part. The male part, an aluminum block, is mounted on the CS, and the female part, a rubber shock absorber, is installed on the FS. There is an adjustable gap between the male and female couplers with a nominal distance of 0.5 mm. The CS is driven by a rotary motor (utilizing transmission gears) mounted on the ground, with a force F_{RM} , so residual vibrations are lowered by channeling the assist force to the ground instead of to the isolated base. The reason to use a rotary motor to drive

CS is that it is energy efficient, creating much less amount of unwanted heat than a linear motor with the same force scale. Thus, using a rotary motor greatly mitigates the step stage's thermal errors. However, because of the backlash present in the transmission gears, it's not accurate enough for conducting fine positioning in the FP regions. Therefore, during the FP regions, the FS disengages itself from the CS and it is instead driven by a small linear motor with high positioning accuracy. Since a FP region is so small compared with the whole motion range of a step, heat generated by the small linear motor during the FP is negligible, and isolated base residual vibrations created are minimal. The state space model of the proposed step stage design is given by:

$$\begin{bmatrix} \dot{y}_g \\ y_g \\ \dot{y}_b \\ y_b \\ \dot{y}_c \\ y_c \\ \dot{y}_f \\ y_f \end{bmatrix} = \begin{bmatrix} 0 & -\frac{k_p + k_b + k_g}{m_g} & 0 & \frac{k_b}{m_g} & 0 & \frac{k_p}{m_g} & 0 & 0 \\ 1 & 0 & 0 & 0 & 0 & 0 & 0 & 0 \\ 0 & \frac{k_b}{m_b} & 0 & -\frac{k_b}{m_b} & 0 & 0 & 0 & 0 \\ 0 & 0 & 1 & 0 & 0 & 0 & 0 & 0 \\ 0 & \frac{k_p}{m_c} & 0 & 0 & 0 & -\frac{k_c + k_b}{m_c} & 0 & \frac{k_c}{m_c} \\ 0 & 0 & 0 & 0 & 1 & 0 & 0 & 0 \\ 0 & 0 & 0 & 0 & 0 & \frac{k_c}{m_f} & 0 & -\frac{k_c}{m_f} \\ 0 & 0 & 0 & 0 & 0 & 0 & 1 & 0 \end{bmatrix} \begin{bmatrix} \dot{y}_g \\ y_g \\ \dot{y}_b \\ y_b \\ \dot{y}_c \\ y_c \\ \dot{y}_f \\ y_f \end{bmatrix} + \begin{bmatrix} \frac{k_g}{m_g} \\ 0 \\ 0 \\ 0 \\ 0 \\ 0 \\ 0 \\ 0 \end{bmatrix} (y_v) \dots \text{Eq. (2)}.$$

where y_c is the CS displacement, y_f is the FS displacement, m_c is the CS mass, m_f is the FS mass, k_c is the coupler stiffness between the FS and CS.

Dynamics Analysis of Proposed Design

Frequency Domain Evaluation

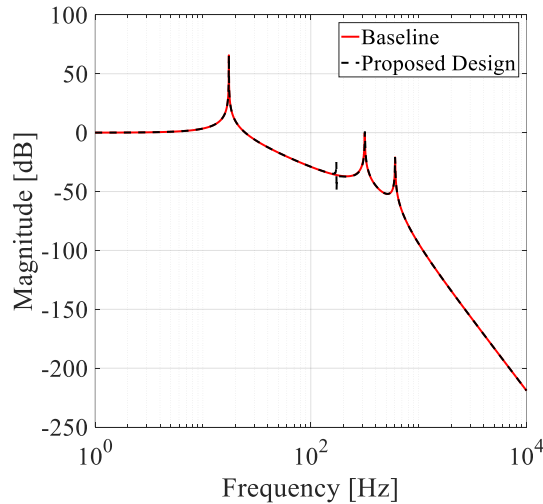


Figure 4. Comparison of ground vibration transmissibility

Figure 4 shows the comparison of the ground vibration transmissibility frequency response functions. The ground vibration transmissibility defined as Y_s / Y_g and Y_F / Y_g for the baseline and proposed design cases, respectively. It is observed that the ground vibration transmissibility of the proposed design is quite similar to that of the baseline design, because both frequency responses match. Therefore, the vibration isolation system of the proposed design will function as well as that of the baseline design, keeping a good feature from the baseline.

Time Domain Evaluations

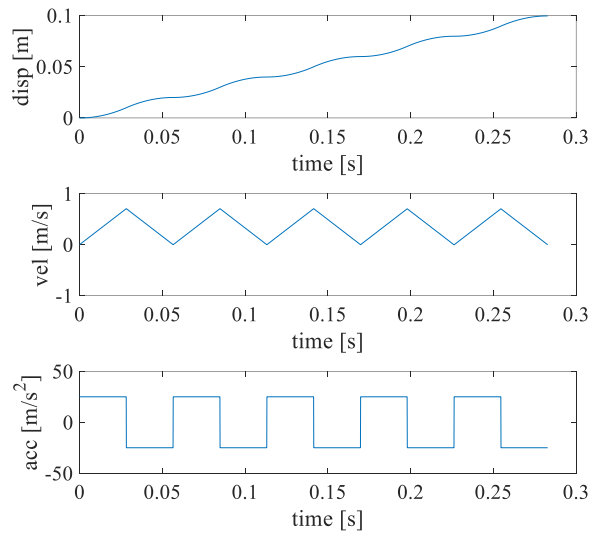


Figure 5. Reference continuous step motion profile of the FS

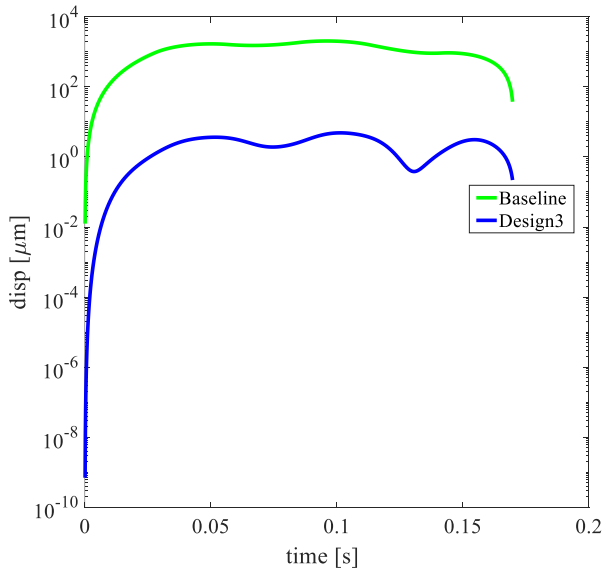


Figure 6a.

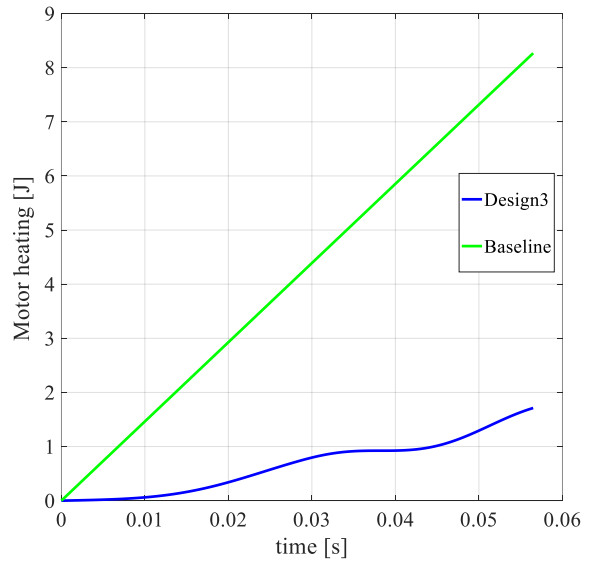


Figure 6b.

Figure 6a shows a semi-log plot for the base vibration comparison, and 6b shows the motor heating comparison.

The reference step profile shown in Figure 5 is used to compare the isolated base vibration of the baseline model, described by Eq. (1), and the proposed design model, described by Eq. (2). The result of the comparison is shown in Figure 6a, and residual base vibrations are reduced by about three orders of magnitude.

The same profile in Figure 5 is also used to compare the motor heat generation of the baseline and the proposed design model. The governing equation for linear motor heat generation is given by:

$$W_{LM} = \int \left(\frac{F_{LM}}{K_{M,LM}} \right)^2 dt \dots \text{Eq. (3)}$$

where F_{LM} is required linear motor force and $K_{M,LM}$ is linear motor constant.

The governing equations for rotary motor torque and heat generation are given by:

$$T_M = a \frac{2\pi S.F.}{\eta l_s} \left(m \frac{l_s^2}{4\pi^2} + J_M \right) \dots \text{Eq. (4)}$$

$$W_{RM} = \int \left(\frac{T_M}{K_{M,RM}} \right)^2 dt \dots \text{Eq. (5)}$$

where a is the step stage acceleration, η is motor efficiency, l_s is step size, m is stage mass, J_M is moment of inertia of the motor, and $K_{M,RM}$ is rotary motor constant. The result of the comparison is shown in Figure 6b. During the 0.28 s motion (5 steps), as for the baseline model, the RMS motor heat generation per step is 8.3 J. However, the new design RMS heat generation per step drops to 1.7 J, indicating 80% reduction.

Prototype Design

Prototype Step Stage Design

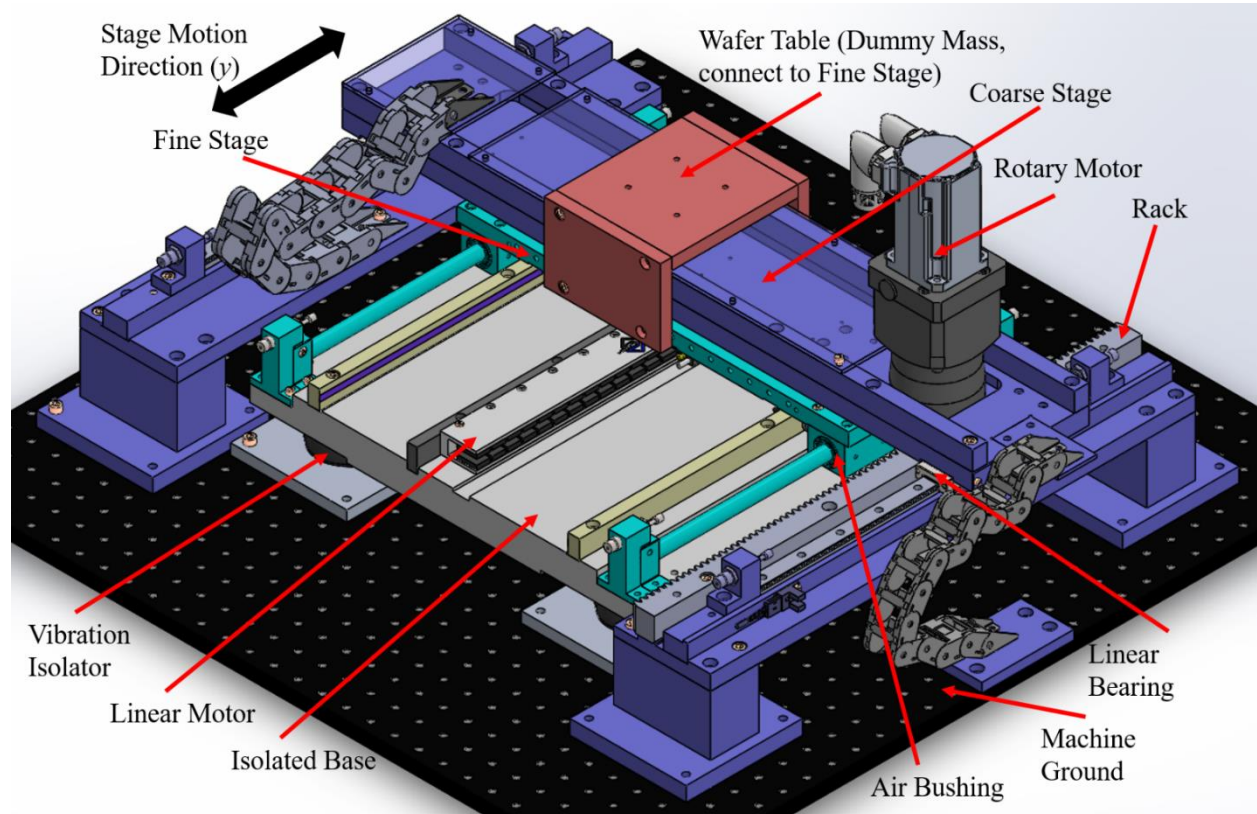


Figure 7. Isometric CAD view of the proposed stage design prototype

Specification	Design Target
Travel Range	180 mm
Max. Acceleration	2.5 g
Max. Speed	1 m/s
Payload	1 kg
Moving Mass	≈ 8.5 kg

Table 1. Prototype design targets

A scale prototype step stage for silicon wafer scanners is designed according to the proposed design concept described in the Design Concept section. Figure 7 shows the CAD model of the prototype. The wafer table (implemented as a dummy mass because only the stepping axis is to be constructed for the scale prototype) is mounted on the FS. The FS is guided by a pair of air bushings (New Way Air Bearings, S301301), each riding on a 13mm precision solid shaft. The FS is mounted on a 400 mm × 400 mm × 33 mm steel base plate suspended by four vibration isolators (Vibrasystem, LF 6045). During the FP regions, the FS is only driven by a high resolution linear motor (Aerotech, BLMUC-95-A-NC-H-S-750), which can provide 161.9 N peak force and 23.0 N

continuous force (no forced cooling condition). During the most of time of a step motion (Acc, CV, and Dcc regions), the FS is carried by the CS, which is guided by a pair of precision-grade linear bearings (Misumi, SSEBZ13) and is driven by a gearbox (10:1 gear ratio) integrated rotary motor with a rack and pinion system with pitch diameter of 34mm (Stöber, ZV217GEPE311SPR0100MA). The gearbox-motor assembly can provide 4.32 N-m continuous and 13.23 N-m peak torque, respectively. The CS is mounted on the machine ground without connection to the isolated base via two aluminum gantries, allowing the rotary motor induced force to be channeled to the ground without disturbing the positioning performance of the FS. The wafer table (or FS) position is measured using an optical linear encoder (Renishaw, RGSZ20), and CS position is measured by a built-in sine encoder of the rotary motor.

Detailed Design Features

1. Coupling Mechanism between the CS and the FS

Figure 8 demonstrates the coupling mechanism in detail. The male coupler is installed on the CS, and it is inserted into the slot on the FS. When the CS and FS engage during Acc, CV, and Dcc regions, the male coupler keeps contacting with the rubber bumper installed on FS, and then FS is either carried or hindered by CS. The nominal clearance between the couplers is 0.5 mm, which provides the 1 mm combined clearance when the FS is pushed against the CS. When the two stages are disengaged from each other, the combined 1 mm clearance provides the fine positioning room for the FS using the linear motor.

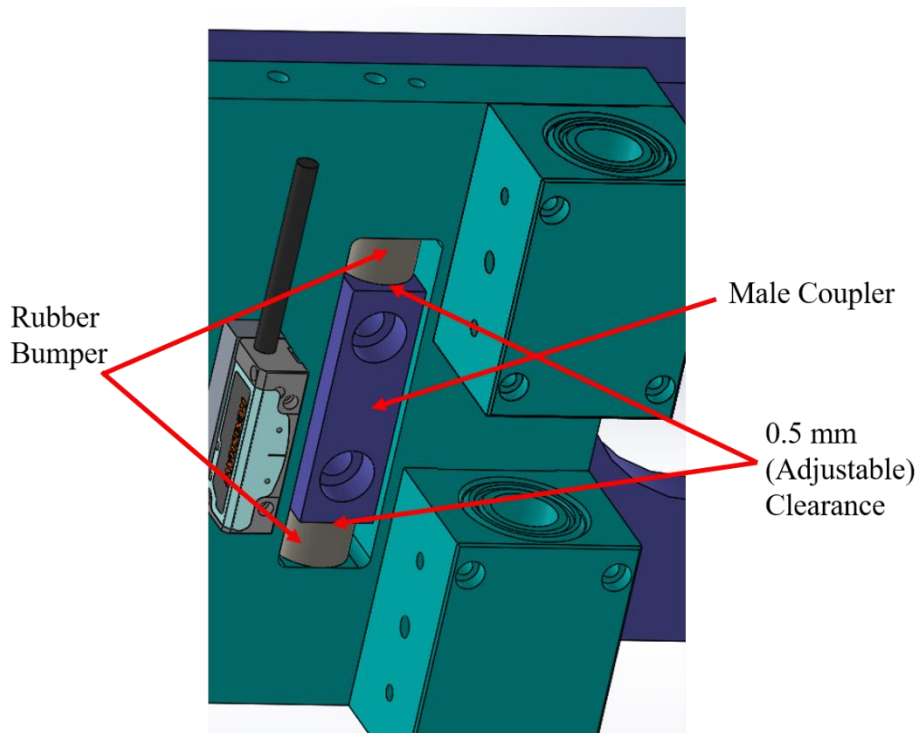


Figure 8. Coupling mechanism between CS and FS

2. Minimum Pitching of the FS

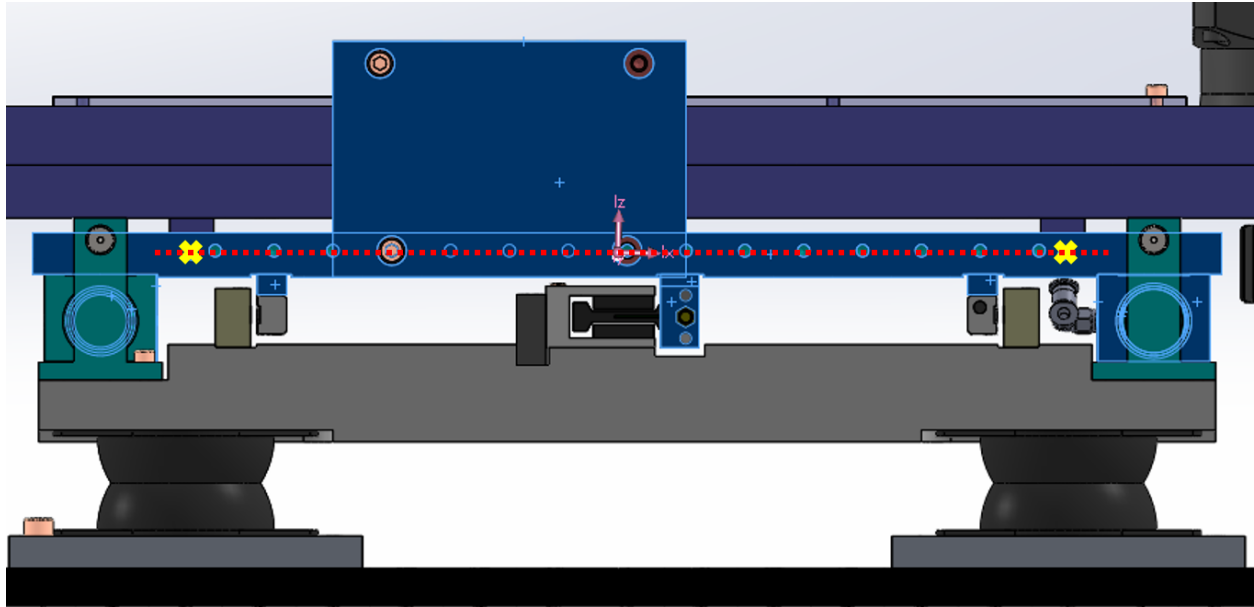


Figure 9. Side view of the prototype CAD drawing

As shown in Figure 9, the center of mass of FS and the wafer table (shown as a pink coordinate) is in line with the center of two couplers (shown as yellow crosses). With this design, in Acc, CV, and Dcc regions, when CS is carrying the FS, there is minimal total moment (pitch) generated on FS. Otherwise, the contact force between the FS and the CS creates a pitch motion of the FS and the base, compromising the fine stage precision accuracy in FP regions.

3. Finite Element Analysis (FEA)

Both static and frequency finite element analyses are run on the FS and FS design. The static FEA ensures the structure of the FS and CS will not fail by yielding. Figure 10a and b show an example of static FEA for simulating an air bushing shaft under the gravitational load of the FS and the wafer table. As shown in Figure 10a, even in the worst scenario, where FS is riding on the center position of the shaft, there is no yielding position. In addition, the slope of the bent shaft is verified to be much smaller than the dimension tolerance of air bushings assembly, as shown in Figure 10b.

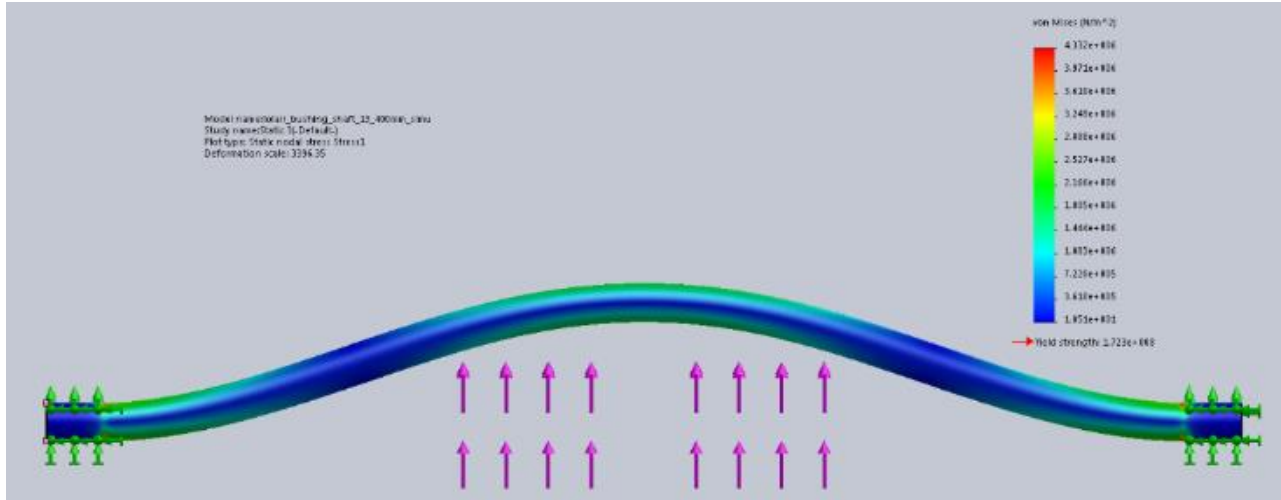


Figure 10a. Stress FEA of the air busing shaft

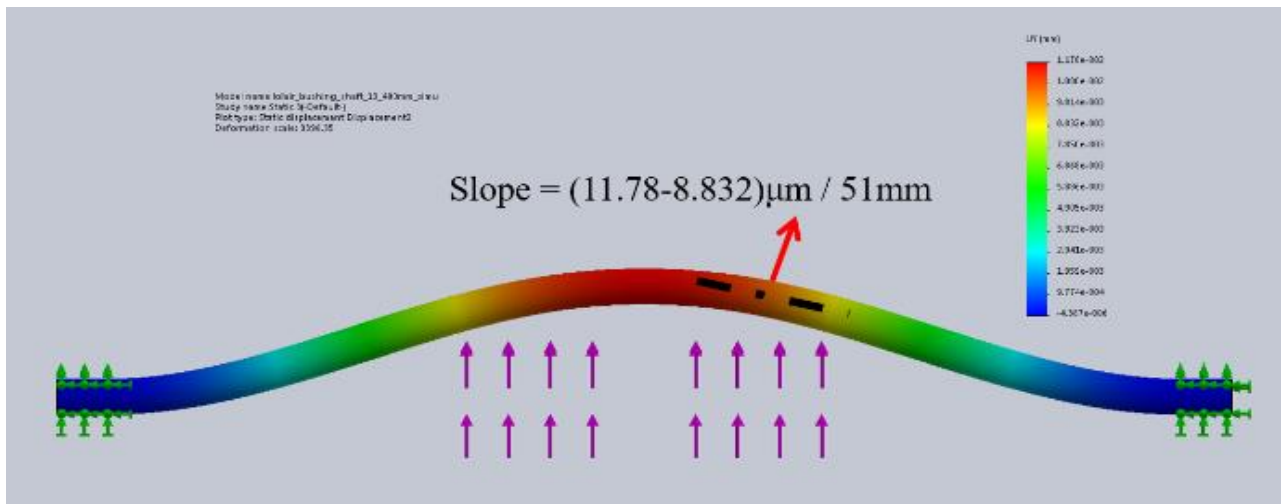


Figure 10b. Deformation FEA of the air busing shaft

Frequency FEA is used to fine-tune the structure of the coarse stage, so as to maximize its 1st eigenfrequencies, thus ensuring high controller bandwidth. The 1st eigenfrequency can be approximated by:

$$\omega_e = \sqrt{\frac{k_{eq}}{m_{eq}}} \dots \text{Eq. (6)}.$$

where k_{eq} is the equivalent stiffness of the structure, and m_{eq} is the equivalent total mass of the structure. The general guide for tuning the structure to have higher eigenfrequency is to increase its relative stiffness. For instance, as shown in Figure 11 and 12, in order to increase CS relative stiffness, two ribs, two sheet metal covers, and a hollowed feature are incorporated into the CS design, ensuring 1st eigenfrequency higher than 450 Hz.

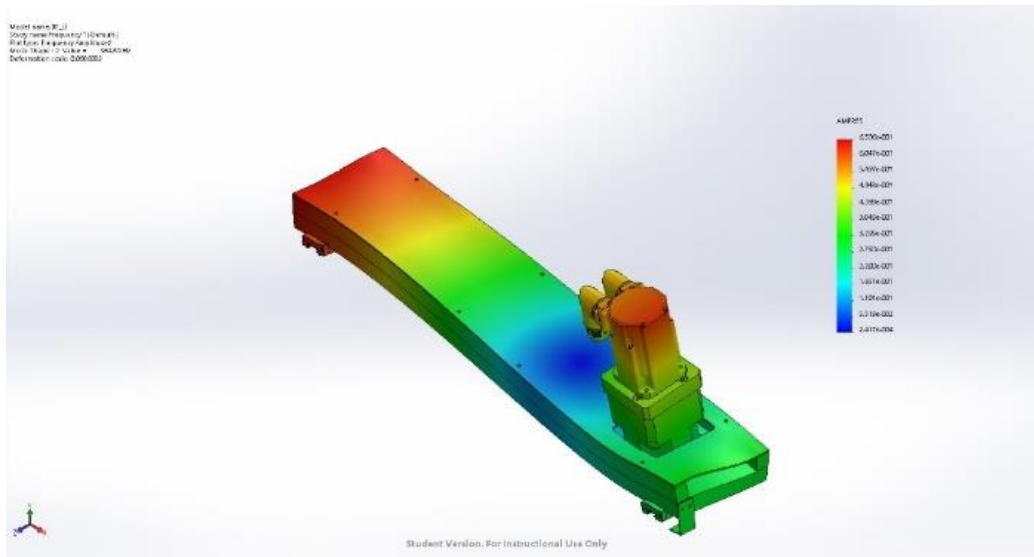


Figure 11. Frequency FEA of CS assembly

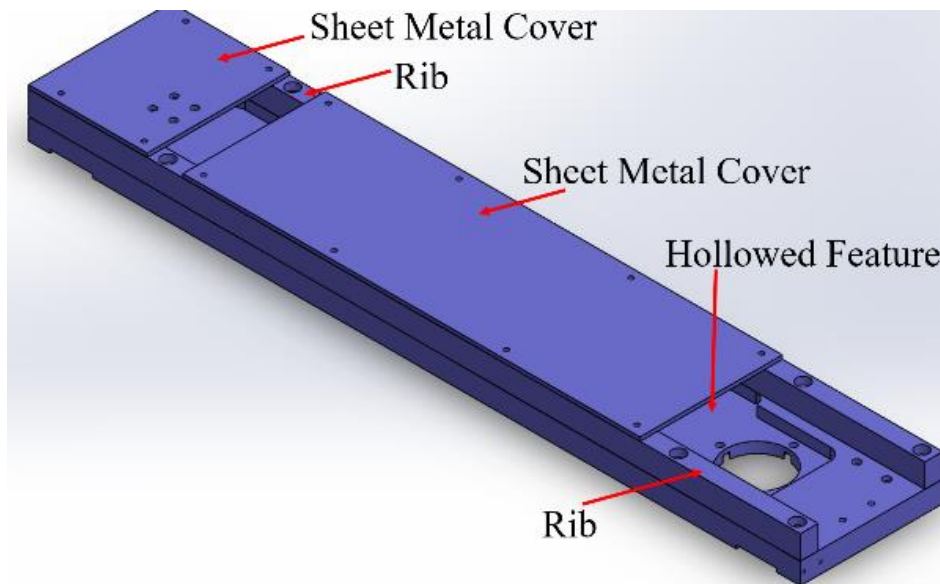


Figure 12. CS structural design features based on the frequency FEA results

Prototype Construction

Figure 13 shows the assembled step stage prototype. All the structural parts are machined by CNC milling machines. Parts that are chunky, and with tight tolerance and highly smooth surface finish requirements (i.e. the black-oxidized steel base, the CS and FS plates, and the gantry top plates) are sent out to LTEK, an Ann Arbor commercial machine shop. The other smaller and simpler parts are manufactured by our own via (Milltronics, VKM 4) milling machines.

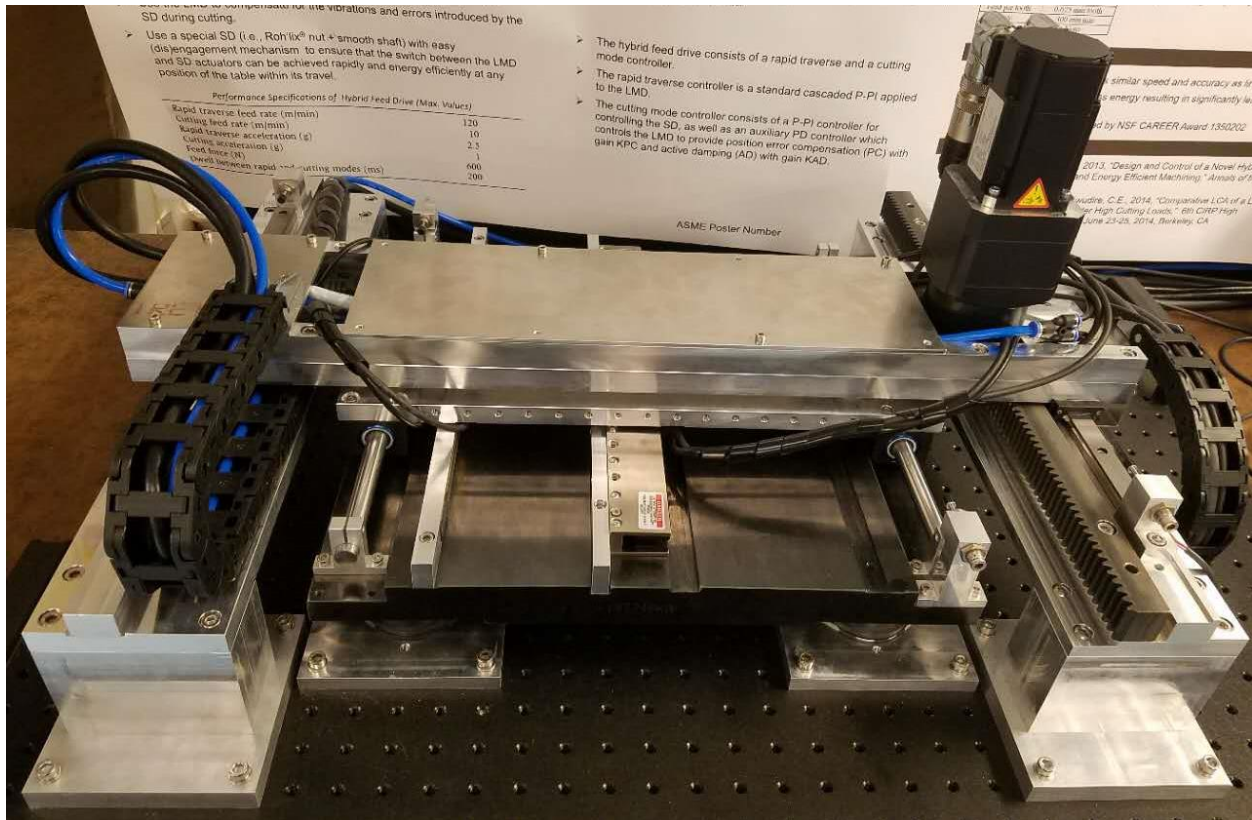


Figure 13. Step Stage Prototype Assembly

Machining Challenges

During the CNC machining process for the step stage prototype, multiple challenges were encountered, and their root-causes and solutions were investigated.

1. Calibrating a milling machine before executing an automated CNC program

Most of the parts were machined (semi-)automatically by executing CNC programs, especially when drilling patterned holes and conducting face cycling to large flat surface areas. However, as shown in Figure 14 when using a CNC program to automatically drill all three counterbore holes on the linear motor mounting block's dimension, the vice misalignment, and the CNC machine's tracking performance, the root-cause was found to be the poor calibration of the CNC machine's encoders. Therefore, before using an unfamiliar CNC machine, it is a good habit to check its calibrations, and to home it on a regular basis.



Figure 14. A misaligned hole at the linear encoder code rail mounting block

2. Mitigation of ripples in parts surface finish

As shown in Figure 15 and 16, at the beginning of the manufacturing process, due to inexperience of the VKM 4 milling machine, it was common to notice obvious ripples on the surface of parts. Surface ripples are caused by three main issues: 1) high feed speed, 2) milling tool wearing, and 3) thin parts (i.e., sheet metal) vibration. A suitable milling feed rate should be adaptively chosen based on the material, cutting depth, and width. It is also suggested to check whether a milling tool's edge is worn or not, before installing it on a milling machine. In addition, while milling a part which has large amount of material cannot be secured by a vise, it is significant to clamp the part together with a supporter, which can support most of the un-vised portion; also, wisely choosing a milling direction so that the cutting force applied to the part is pointing towards the supporter, instead of pointing out of the supporter, is important.

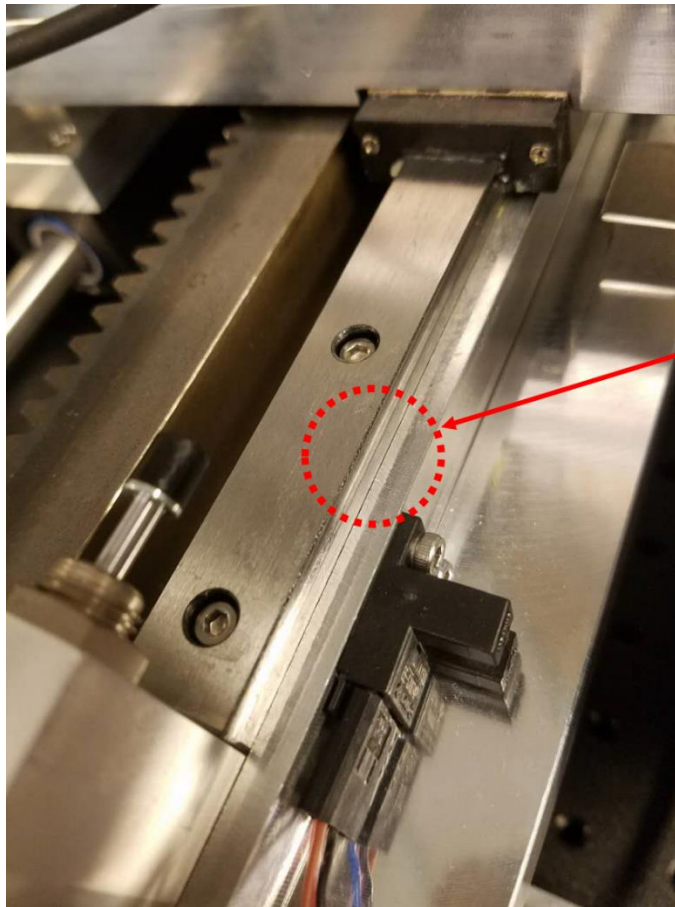


Figure 15. Surface ripples on the gantry support block



Figure 16. Surface ripples on the linear motor mounting block

After accomplishing all manufacturing tasks for the step stage prototype, the prototype was assembled according to the assembly plan. Using machined plane to align parts is the major method adopted to ensure high position accuracy in assembly. Figure 17 shows how the linear bearing rail is aligned with the gantry rib with machined plane on the side. Figure 18 shows how the optical encoder mounting block is aligned to FS with the machined plane. The same practice is implemented on a number of parts assembled on the gantry top plate, the isolated base, CS, FS, etc.



Linear bearing rail and gantry rib touching at the machined plane

Figure 17. Linear bearing rail and gantry rib touching at the machined plane



Encoder mounting block and FS touching at the machined plane

Figure 18. Encoder mounting block and FS touching at the machined plane

Design for Assembly

Several design mistakes were found out during the assembling process, which provided further guidance of how to apply the principle of design for assembly (DFA), when designing a machine in general.

1. Check accessibility of tools to assembling locations

Figure 19 shows that one screw to fasten the vibration isolator mounting block cannot be installed because an allen wrench cannot reach that location. Therefore, before designating a fastener location, it is important to check whether the tool will have access to the designed location.

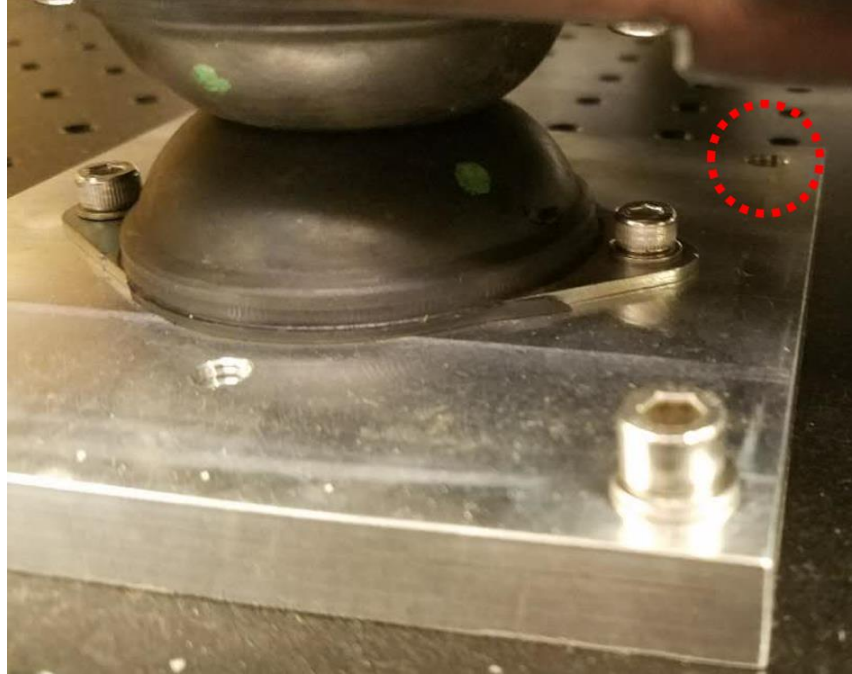


Figure 19. An allen wrench cannot reach the screw clearance hole on the isolator mounting block

2. Check easiness to adjust parts

After assembling, some components of the step stage need to be disassembled and recalibrated such as the optical encoder. Since the optical encoder is mounted on the FS, and the FS is covered by the CS, it is difficult to calibrate it without removing the CS. Therefore, as shown in Figure 20, two holes are created on the CS, so that an allen wrench can easily reach the screws of the encoder on the FS without removing the CS.

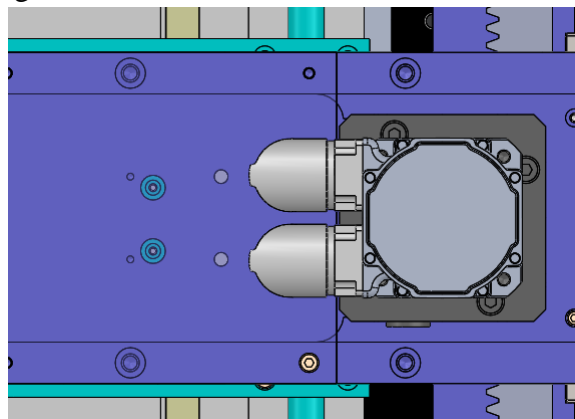


Figure 20. Clearance holes to facilitate the optical encoder calibration

Summary and Future Work

In this work, a new design approach for increasing the throughput of the step stage for silicon wafer scanners is presented. By using a coarse and fine step stage configuration, the new design can simultaneously mitigate motor heating and stage vibration, so as to increase the stage throughput. The model based simulations show that the new design is expected to provide an excellent performance compared with a baseline stage design. A scale prototype of the proposed design is designed and built. Future work will investigate control architectures of the stage and validate the effectiveness of the stage design.

Reference

- [1] Lu C, Tsai D. Independent Component Analysis-Based Defect Detection in Patterned Liquid Crystal Display Surfaces. *Image and Vision Computing*. 2008; 26: 955-970.
- [2] Butler H. Position Control in Lithographic Equipment. *IEEE Control Systems*. 2011; 31: 28-47.
- [8] Erkorkmaz K, Gorniak J, Gordon D. Precision Machine Tool X–Y Stage Utilizing a Planar Air Bearing Arrangement. *CIRP Annals-Manufacturing Technology*. 2010; 59: 425-428.
- [3] Rivin E. Vibration Isolation of Precision Equipment. *Precision Engineering*. 1995; 17: 41-56.
- [4] Okwudire C, Lee J. Minimization of the Residual Vibrations of Ultra-Precision Manufacturing Machines via Optimal Placement of Vibration Isolators. *Precision Engineering*. 2013; 37: 425-432.
- [6] Yoon D, Okwudire CE. Magnet Assisted Stage for Vibration and Heat Reduction in Wafer Scanning. *CIRP Annals - Manufacturing Technology*. 2015; 64: 381-384.